Neutron physics of the Re/Os clock:
Paper I. Measurement of the (n,γ) cross sections of ^{186,187,188}Os at CERN n_TOF

M. Mosconi[1], K. Fujii[2], A. Mengoni[3,17] C. Domingo-Pardo[1,4], F. Käppeler[1], U. Abbondanno[2], G. Aerts[5],
H. Álvarez-Pol[6], F. Alvarez-Velarde[7], S. Andriamonje[5], J. Andrzejewski[8], P. Assimakopoulos [9],
L. Audouin [1], G. Badurek[10], P. Baumann[11], F. Bečvář[12], F. Belloni[2], E. Berthoumieux[5], S. Bisterzo[1,13],
M. Calviani[14], F. Calviño[15], D. Cano-Ott[7], R. Capote[3,16], A. Carrillo de Albornoz[17], P. Cennini[18],
V. Chepel[19], E. Chiaveri[18], N. Colonna[20], G. Cortes[15], A. Couture[21], J. Cox[21], M. Dahlfors[18], S. David[22],
I. Dillmann[1], R. Dolfini[23], W. Dridi[5], I. Duran[6], C. Eleftheriadis[24], M. Embid-Segura[7], L. Ferrant[22],
A. Ferrari[18], R. Ferreira-Marques[19], L. Fitzpatrick[18], H. Frais-Koelbl[3], W. Furman[25], R. Gallino[13],
I. Goncalves[19], E. Gonzalez-Romero[7], A. Goverdovski[26], F. Gramegna[14], E. Griesmayer[3], C. Guerrero[7],
F. Gunsing[5], B. Haas[27], R. Haight[28], M. Heil[1], A. Herrera-Martinez[18], M. Igashira[29], S. Isaev[22], E. Jericha[10],
Y. Kadi[18], D. Karamanis[9], D. Karadimos[9], M. Kerveno,[11], V. Ketlerov[25,17], P. Koehler[30], V. Konovalov[24,17],
E. Kossionides[31], M. Krtička[12], C. Lamboudis[9], H. Leeb[10], A. Lindote[19], I. Lopes[19], M. Lozano[16],
S. Lukic[11], J. Marganiec[8], L. Marques[17], S. Marrone[20], C. Massimi[32], P. Mastinu[14], P.M. Milazzo[2],
C. Moreau[2], F. Neves[19], H. Oberhummer[10], M. Oshima[33], S. O'Brien[21], J. Pancin[5], C. Papachristodoulou[9],
C. Papadopoulos[34], C. Paradela[6], N. Patronis[9], A. Pavlik[35], P. Pavlopoulos[36], L. Perrot[5], R. Plag[1], A. Plompen[37],
A. Plukis[5], A. Poch[15], C. Pretel[15], J. Quesada[16], T. Rauscher[38], R. Reifarth[28], M. Rosetti[39], C. Rubbia[23],
G. Rudolf[11], P. Rullhusen[37], J. Salgado[17], L. Sarchiapone[18], I. Savvidis[24], C. Stephan[22], G. Tagliente[20],
J.L. Tain[4], L. Tassan-Got[22], L. Tavora[17], R. Terlizzi[20], G. Vannini[32], P. Vaz[17], A. Ventura[39], D. Villamarin[7],
M. C. Vincente[7], V. Vlachoudis[18], R. Vlastou[34], F. Voss[1], S. Walter[1], H. Wendler[18], M. Wiescher[21], K. Wisshak[1]

The n_TOF Collaboration

[1]*Karlsruhe Institute of Technology (KIT), Campus Nord,
Institut für Kernphysik, Germany;* [2]*Istituto Nazionale di Fisica Nucleare,
Trieste, Italy;* [3]*International Atomic Energy Agency,
NAPC-Nuclear Data Section, Vienna, Austria;* [4]*Instituto de Física Corpuscular,
CSIC-Universidad de Valencia, Spain;* [5]*CEA/Saclay - DSM,
Gif-sur-Yvette, France;* [6]*Universidade de Santiago de Compostela,
Spain;* [7]*Centro de Investigaciones Energeticas Medioambientales y Technologicas,
Madrid, Spain;* [8]*University of Lodz, Lodz, Poland;* [9]*University of Ioannina,
Greece;* [10]*Atominstitut der Österreichischen Universitäten,Technische Universität Wien,
Austria;* [11]*Centre National de la Recherche Scientifique/IN2P3 - IReS,
Strasbourg, France;* [12]*Charles University, Prague,
Czech Republic;* [13]*Dipartimento di Fisica Generale, Università di Torino,
Italy;* [14]*Istituto Nazionale di Fisica Nucleare(INFN), Laboratori Nazionali di Legnaro,
Italy;* [15]*Universitat Politecnica de Catalunya, Barcelona, Spain;* [16]*Universidad de Sevilla,
Spain;* [17]*Instituto Tecnológico e Nuclear(ITN), Lisbon, Portugal;* [18]*CERN, Geneva,
Switzerland;* [19]*LIP - Coimbra & Departamento de Fisica da Universidade de Coimbra,
Portugal;* [20]*Istituto Nazionale di Fisica Nucleare,
Bari, Italy;* [21]*University of Notre Dame, Notre Dame,
USA;* [22]*Centre National de la Recherche Scientifique/IN2P3 - IPN, Orsay,
France;* [23]*Università degli Studi Pavia, Pavia, Italy;* [24]*Aristotle University of Thessaloniki,
Greece;* [25]*Joint Institute for Nuclear Research, Frank Laboratory of Neutron Physics,
Dubna, Russia;* [26]*Institute of Physics and Power Engineering, Kaluga region,
Obninsk, Russia;* [27]*Centre National de la Recherche Scientifique/IN2P3 - CENBG,
Bordeaux, France;* [28]*Los Alamos National Laboratory,
New Mexico, USA;* [29]*Tokyo Institute of Technology, Tokyo,
Japan;* [30]*Oak Ridge National Laboratory, Physics Division,
Oak Ridge, USA;* [31]*NCSR, Athens, Greece;* [32]*Dipartimento di Fisica,
Università di Bologna, and Sezione INFN di Bologna,
Italy;* [33]*Japan Atomic Energy Research Institute, Tokai-mura,
Japan;* [34]*National Technical University of Athens,
Greece;* [35]*Faculty of Physics, University of Vienna,
Austria;* [36]*Pôle Universitaire Léonard de Vinci,
Paris La Défense, France;* [37]*CEC-JRC-IRMM, Geel,
Belgium;* [38]*Department of Physics and Astronomy - University of Basel,*

Basel, Switzerland; [39]*ENEA, Bologna, Italy.* *
(Dated: May 12, 2010)

The precise determination of the neutron capture cross sections of ^{186}Os and ^{187}Os is important to define the s process abundance of ^{187}Os at the formation of the solar system. This quantity can be used to evaluate the radiogenic component of the abundance of ^{187}Os due to the decay of the unstable ^{187}Re ($t_{1/2} = 41.2$ Gyr) and from this to infer the time-duration of the nucleosynthesis in our galaxy (Re/Os cosmochronometer). The neutron capture cross sections of ^{186}Os, ^{187}Os, and ^{188}Os have been measured at the CERN n_TOF facility from 1 eV to 1 MeV, covering the entire energy range of astrophysical interest. The measurement has been performed by time-of-flight technique using isotopically enriched samples and two C_6D_6 scintillation detectors for recording the prompt γ-rays emitted in the capture events. Maxwellian averaged capture cross sections have been determined for thermal energies between $kT = 5$ and 100 keV corresponding to all possible s-process scenarios. The estimated uncertainties for the values at 30 keV are 4.1, 3.3, and 4.7 % for ^{186}Os, ^{187}Os, and ^{188}Os respectively.

I. INTRODUCTION

The long half-life of 41.2 Gyr [1] makes ^{187}Re an important potential cosmo-chronometer. Originally proposed by Clayton [2], this chronometer is particularly appealing because ^{187}Re can be attributed to the r process, which is believed to occur in supernova explosions of massive stars. Since these stars evolve quickly, the clock started early after galaxy formation. This was confirmed by recent observations of very metal poor stars, which exhibit remarkably consistent r-process abundance patterns [3–5]. Another important feature of this clock is that it can be almost completely analyzed in terms of the nuclear properties of the mother/daughter pair ^{187}Re/^{187}Os. Therefore, it represents a valuable independent complement to other dating methods based on astronomical observations, i.e. for deriving the Hubble age [6], globular cluster ages [7], or age estimates from analyses of the cosmic microwave background [8].

The idea of the Re/Os clock is sketched in Fig. 1, which shows the reaction paths in the W-Re-Os region. Abundance contributions from the r-process region are indicated by dashed arrows. The main s-process flow is sketched by solid lines, indicating the network of (n,γ) reactions and β decays. The unstable isotopes ^{185}W and ^{186}Re (circles) represent branching points for the reaction flow, because their half lives are sufficiently long for neutron capture to compete with β decays. If these branchings were negligible, ^{187}Re could be considered as a pure r-only isotope, which is shielding ^{187}Os from the r-process beta decay chains. Therefore, the radiogenic contribution to the abundance of ^{187}Os could be determined by subtraction of the s-process component from the observed abundance value. The branchings at ^{185}W and ^{186}Re require a corresponding correction of the radiogenic component, which can be determined by a detailed analysis of the s-process reaction flow using a reliable set

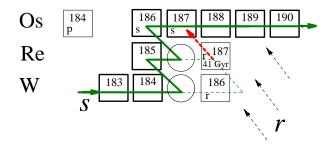of stellar (n,γ) cross sections [9–11].

FIG. 1: (Color online) The reaction path of the s process in the W-Re-Os region. The main s process flow is sketched by solid lines, circles correspond to branchings in the s path, and r-process contributions from explosive nucleosynthesis are indicated by dashed arrows. The decay of ^{187}Re constitutes a cosmo-chronometer, which can be analyzed because the radiogenic component of ^{187}Os can be determined by subtraction of the s-process component. This s component is defined by the abundance of the s-only nucleus ^{186}Os via s-process systematics.

Problems related to the Re/Os clock (apart from a realistic model of galactic chemical evolution) were found to originate from the dramatic temperature dependence of the ^{187}Re half-life, a possible minor s-process contribution to ^{187}Re, and a sizable correction for the s-process abundance of ^{187}Os due to thermal population of low-lying excited nuclear states. The first issue could be settled by a measurement of the half-life of fully stripped ^{187}Re atoms [12] and by subsequent analyses, which demonstrated that the astration effect related to the destruction of ^{187}Re in later stellar generations is not crucial for the reliability of the clock [13]. Similarly, the s-process contributions to ^{187}Re due to the branchings at ^{185}W and ^{186}Re were shown to have no significant impact either [9, 11, 14].

The remaining nuclear issues, which need to be addressed for the improvement of the Re/Os clock, refer to the determination of more accurate Maxwellian aver-

aged cross sections (MACS) for neutron capture on ^{186}Os and ^{187}Os. This information is required for defining the s-process contribution to ^{187}Os via the local approximation, $\langle\sigma\rangle\,N_s$ = constant, which is well satisfied in this mass region. Because ^{186}Os is exclusively produced by the s process, the s component of ^{187}Os is given by

$$N_{s,187} = \frac{\langle\sigma\rangle_{186}}{\langle\sigma\rangle_{187}}\,N_{s,186} \qquad (1)$$

where $\langle\sigma\rangle_i$ are the MACSs that can in principle be calculated from experimentally measured (n,γ) cross sections with only a small correction of 0.4% for the fact that the s-process reaction chain in the Os region is almost but not completely in flow equilibrium.

Under stellar conditions, however, the MACS derived from laboratory data must be corrected for the effect of thermally populated excited states. The contribution of captures by the excited states have to be obtained by theoretical calculations. The corresponding corrections are the stellar enhancement factors (SEF). In these calculations, additional knowledge of the inelastic cross section is important to constrain the effect of superelastic scattering by the excited states, where neutrons gain in energy if the final state is lower in energy than the initial one. The stellar enhancement effect is particularly important for ^{187}Os, where low-lying nuclear states at 9.75, 74.3, 75.0 and 100.6 keV have to be considered. In ^{186}Os, the SEF is much smaller, because only the first excited state at 137.2 keV, which is considerably less populated, contributes to the SEF correction.

Previous measurements of the (n,γ) cross sections for ^{186,187}Os were reported in limited energy ranges only, from 2.75 keV to 2.65 MeV [15], from 1 to 135 keV [16], and from 5 to 90 keV [17]. Below 1 keV, experimental information is rather incomplete [18], leading to large uncertainties in the MACSs at the low thermal energies typical of the s process during the interpulse phases of asymptotic giant branch (AGB) stars [19]. The MACS at low thermal energies are particularly important because the interpulse phase contributes most of the s-process neutron exposure via the ^{13}C$(\alpha,n)^{16}$O reaction [20]. Among the available cross section sets, the MACSs of ^{186}Os exhibit some discrepancies, especially at energies close to the first excited state of ^{186}Os at 130 keV, where a pronounced step in the cross section is expected. Consequently, improved capture cross section measurements were required to resolve existing discrepancies and to extend the energy range to lower and higher energies.

In addition, the available measurements of the inelastic scattering cross section of ^{187}Os [21–24] exhibit large uncertainties that are limiting the reliability of the SEF calculations and have a serious effect on the Re/Os age. Therefore, an accurate independent measurement of the (n,n') cross section of ^{187}Os is called for as well. Finally, refined resonance analyses are important to obtain a consistent set of level densities as well as neutron and γ-ray strength functions for the cross section calculation of excited states and the related determination of reliable values for the SEFs.

This complex of information was obtained in high-resolution measurements of (n,γ) cross sections for ^{186,187,188}Os at the CERN n_TOF facility reported in this contribution (Paper I). In a second experiment the neutron inelastic scattering cross section was determined at the Karlsruhe 3.7 MV Van de Graaff accelerator (Paper II). In addition, detailed resonance analyses of the n_TOF capture data were performed and used together with the (n,n') data for improved SEF calculations, which were carried out with the Hauser-Feshbach statistical model for an updated assessment of the Re/Os cosmo-chronometer (Paper III).

II. MEASUREMENT

A. The n_TOF facility

At n_TOF, neutrons are produced by spallation of 20 GeV/c protons on a massive lead target. The beam is delivered by the proton synchrotron accelerator (PS) of the CERN complex in bunches of 4 to 7×10^{12} protons, with a pulse width of 7 ns and typical repetition frequency of 0.4 Hz. About 300 neutrons/proton are produced by the spallation module. The experimental area is 185 m away from the target station, allowing for an energy resolution of 5.5×10^{-4} at 1 keV and a flux of the order of 2×10^5 neutrons/pulse/energy decade in the neutron energy range from 1 eV to 1 MeV [25].

Together with the neutrons, a cascade of ultrarelativistic particles are generated in the lead target which could act as a potential source of background. This background is suppressed by massive concrete shielding along the beam line and by a sweeping magnet at 145 m from the spallation target. Photons and the residual relativistic particles generated directly by the proton interactions and traveling inside the beam pipe are easily separated from the neutrons by TOF and the corresponding γ-flash is actually used to mark the time zero point in the TOF spectrum.

Most critical are photons generated by neutron capture in the material surrounding the target, in particular by hydrogen of the cooling water. These photons are mainly produced in the interval from 1 μs to a few 100 μs after the proton pulse hits the target and arrive in the experimental area together with the neutrons of energies in the keV range. The background produced by Compton scattering of these photons in the sample is significant and requires careful subtraction. A set of removable neutron filters of aluminum, tungsten, molidenum, silver, and cobalt at 135 m from the target is used for measuring this background at the energies of so-called black resonances, which are large enough that all neutrons of that energy are removed from the beam.

B. Experimental setup

In the present measurement, the experimental setup consisted of two C_6D_6 scintillation counters and a set of samples mounted on the ladder of an automatic sample changer as shown in Fig. 2.
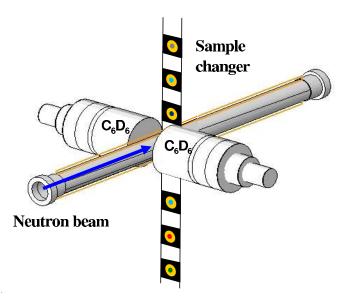

FIG. 2: (Color online) Sketch of sample changer and detectors in the experimental area at a flight path of 185 m.

The detectors were designed for the lowest possible neutron sensitivity in order to avoid time-correlated background from neutrons scattered in the samples [26]. This was achieved by using a very light scintillator cell of carbon fiber that was directly glued onto the photomultiplier, thus minimizing the detector materials. To reduce the background due to in-beam γ-rays from neutron captures in the water moderator [25], which are scattered by the samples preferentially in forward direction, the detectors were mounted 9.5 cm upstream of the samples.

Similarly, the sample changer was designed to avoid background from scattered neutrons. It consisted essentially of a ladder made from a carbon fiber strip for holding the samples. The sample changer was remotely operated by a stepping motor. The evacuated beam pipes were stainless steel tubes (wall thickness 0.5 mm) with 25 μm thick Kapton$^{©}$ windows.

A neutron monitor consisting of a ^{6}Li layer 200 μg/cm^2 in thickness evaporated onto a 1.5 μm thick Mylar foil was mounted about 3.5 m upstream of the capture samples for additional flux measurements [27]. The products of the ^{6}Li$(n, \alpha)^3$H reaction were recorded by four silicon crystals surrounding the ^{6}Li foil outside the neutron beam.

In total six samples were used in the measurement, the ^{186,187,188}Os isotopes under study, a ^{197}Au sample for flux normalization, natural carbon and lead samples for determining the backgrounds due to scattered neutrons, and in-beam γ-rays, and an empty container to correct for the capture events in the aluminum. An empty position on the sample changer served for measuring the ambient background. The osmium samples consisted of enriched metal powder encapsulated in 0.1 mm thick aluminum cans 15 mm in diameter. The sample characteristics are summarized in Table I.

C. Data acquisition

The detector signals have been recorded with fast digitizers at a sampling rate of 500 MHz corresponding to time steps of 2 ns/Sample. Triggered by the pick-up signal of the accelerator, each neutron burst could be followed for 16 ms by intermediate data storage in the 8 MByte on-board memory of the digitizers. The neutron energies covered in capture measurements with C_6D_6 detectors was limited to a maximum of about 1 MeV due to the opening of inelastic channels and to a minimum of 0.7 eV due to the 16 ms time interval provided by the storage capacity of the digitizers. The time zero point in the TOF spectrum was derived from the γ-flash. For events following the γ-flash, TOF, pulse height, and integrated charge were determined by an off-line analysis routine. This raw information was converted into pre-processed data by energy calibration of the scintillators, verification of gain stability, selection of proper thresholds, and rejection of coincident events as described in Ref. [28].

III. DATA ANALYSIS

The data analysis has been divided into the resolved resonance region (RRR) and the continuum part. The parameters of the resolved resonances have been obtained up to neutron energies of 5, 3, and 8 keV for ^{186}Os, ^{187}Os, and ^{188}Os as described in Paper III [29].

The average capture cross sections in the continuum region were analyzed starting at neutron energies slightly below the upper limit of the RRR to check the consistency of the two independent analyses. The cross sections in the continuum have been obtained from the pre-processed capture data after application of the pulse height weighting technique (PHWT), background subtraction, and flux normalization.

A. Pulse height weighting

The experimental capture yields are obtained by applying the PHWT [30], an *a posteriori* manipulation of the detector response to ensure that the γ-ray efficiency increases linearly with the detector signal. This is achieved by means of weighting functions (WF), which are parameterized as polynomial functions of the γ-ray energy. Each recorded detector signal is multiplied with

| Sample | Mass | Thickness | Chemical | Isotopic composition (%) | | | | | |
	[mg]	[10^{-3} atoms/b]	form	186	187	188	189	190	192
^{186}Os	1999.9	3.714	metal powder	78.48	0.91	4.88	4.29	5.09	5.32
^{187}Os	1921.2	3.549	metal powder	1.06	70.43	12.73	5.13	5.42	5.21
^{188}Os	1996.7	3.669	metal powder	0.11	0.12	94.99	2.55	1.27	0.97
Gold	1299.0	2.241	metal	natural					
Lead	2027.0	3.171	metal	natural					
Carbon	479.0	13.48	graphite	natural					

^{a}All samples 15 mm in diameter.

the proper WF to correct for the γ efficiency of the detectors. The absolute efficiency obtained in this way has been verified by comparison with the well known (n, γ) cross section of ^{197}Au at 25 keV as discussed in Sec. III C.

An accuracy of 2% was determined for the PHWT by a detailed study of the possible sources of systematic uncertainties, i.e. related to the corrections for multiple scattering and self shielding [25]. The PHWT requires coincidence rejection, reliable energy calibration of the γ-ray detection, and a detailed simulation of the experimental setup to determine the weighting functions.

The WFs for the osmium and gold samples have been determined independently using the simulation tools MCNP [31] and GEANT3.21 [32]. The related systematic uncertainty was estimated by the differences in the count rates obtained with the two weighting functions, which were 1%, 0.4%, and 0.4% for ^{186}Os, ^{187}Os, and ^{188}Os, respectively. A separate WF for gold, which had been determined with the GEANT4 tool kit, was also reproducing the capture yield to $\leq 1\%$. These systematic uncertainties partly compensate each other, because the Os capture yields are obtained relative to gold.

B. Backgrounds

In the analysis of the osmium and gold spectra, all backgrounds are treated by the PHWT as they were true capture events. Therefore, the events of the lead and carbon samples must be weighted using the same weighting procedure than events from the respective Os sample.

Fig. 3 shows the resulting TOF spectra for the ^{186}Os sample together with the spectra for background determination, which are representative for the energy and time dependence of the background. Only a few narrow capture resonances in the lead spectrum had to be excluded, whereas the 34 keV ^{27}Al resonance in the spectrum of the empty can had to be considered for background subtraction. Apart from that resonance there is no significant difference between the spectra of the empty position and of the empty can. In the astrophysically relevant energy range between 1 and 300 keV one finds that the background is dominated by the contribution from in-beam γ rays.
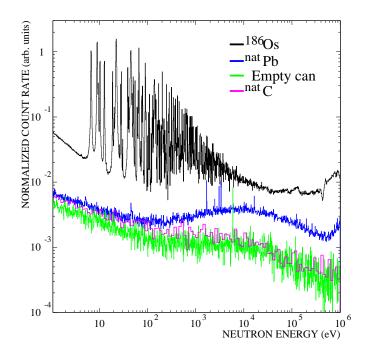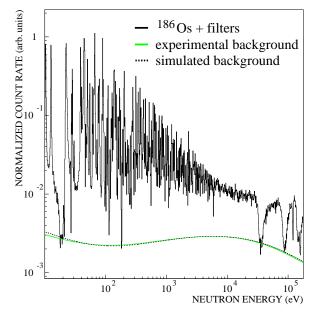

FIG. 3: (Color online) TOF spectrum of ^{186}Os together with the (not yet normalized) spectra for background determination. In the ^{186}Os spectrum the region of resolved resonances extends to several keV. The low neutron sensitivity of the setup is illustrated by the fairly small difference between the spectra taken with the carbon sample and the empty can. the background in the keV region is dominated due to scattering of in-beam γ rays by the sample.

The actual background level is experimentally determined by the contributions measured with the empty position and with the lead and carbon samples. Additional background information was obtained in runs made with black neutron filters and with detailed simulations of the scattering of in-beam γ-rays by the samples. Because the measurements with the filters represent only a few energy points and because the statistics at the bottom of the black resonances is in general poor, Monte Carlo simulations were used to complement these measurements. This technique was successfully applied in other n_TOF measurements as well [33, 34].

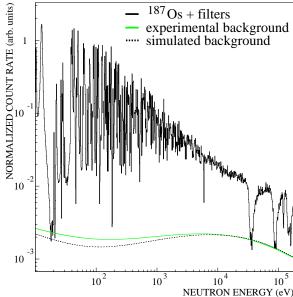An additional background component is due to $(n, n'\gamma)$

FIG. 4: (Color online) Measured and simulated backgrounds plotted as dashed and solid lines. Both results were normalized to match the level at the energies of black resonances at 18 eV (W filter) and at 34 and 90 keV (Al filter).

events in the samples and deuteron recoils in the scintillator. In both cases this background starts to contribute only above 500 keV. Therefore, the analysis was repeated for all Os isotopes using an energy-deposition threshold of 500 keV. These results were then renormalized to the cross sections determined with the common threshold at 200 keV.

The overall background was determined by a polynomial fit of the dominant background components, i.e. of the ambient part represented by the spectra of the empty can and the part due to in-beam γ-rays obtained from the lead spectra. The sum of both components was normalized to match the background level measured with the W and Al neutron filters at 18 eV and at 34 and 90 keV, corrected for the γ-ray absorption in the filters as shown by the dashed lines in Fig. 4.

An independent determination of the neutron- and γ-ray induced backgrounds was performed by Monte Carlo simulations based on the neutron scattering cross sections and on the spectrum of in-beam γ-rays produced near the spallation target [25]. The corresponding interactions with the samples were simulated using GEANT3.21 [35]. The result of the simulation (dotted lines in Fig. 4) is in good agreement with the experimental background. Due to the different signal/background ratios in the spectra of the Os isotopes, the remaining differences in the overall background are affecting the cross sections of ^{186}Os, ^{187}Os, and ^{188}Os by 2%, 1%, and 3% around 30 keV, respectively.

Both approaches were eventually combined to determine the background level with improved accuracy.

C. Absolute neutron flux

A relative normalization of the well defined energy dependence of the neutron flux [27, 36] could be obtained for the various runs via the ^{6}Li neutron monitor. The absolute flux was determined by means of the gold reference sample, using the (n,γ) cross section of ^{197}Au as a standard.

The first gold resonance at 4.9 eV has been used for defining the flux in the RRR using the saturated resonance method [37]. The absolute yield normalization was determined by a fit with the R-matrix code SAMMY [38] and adopting the resonance parameters of Ref. [18]. The background below the first gold resonance is completely negligible compared to the capture signal. In the keV region, the (n,γ) cross section at 25 keV is known with 1.5% uncertainty [39] and is often used as standard in nuclear astrophysics. In this case, however, the background subtraction is crucial, because the signal/background ratio at this energy is about 4, two orders of magnitude lower than for the 4.9 eV resonance.

The background for the Au spectrum was determined analogously to the method applied in case of the Os spectra. An additional verification could be obtained via the independent flux normalizations at 4.9 eV and 25 keV as illustrated in Fig. 5. The normalization at 25 keV resulted in a predicted yield at the top of the 4.9 eV resonance in perfect agreement with the SAMMY fit on the basis of the presently adopted resonance parameters [18].

Although the absolute flux normalization was found in perfect agreement, a systematic uncertainty of 2% has been adopted for the energy dependence of the neutron flux, which has been determined in n_TOF measurements
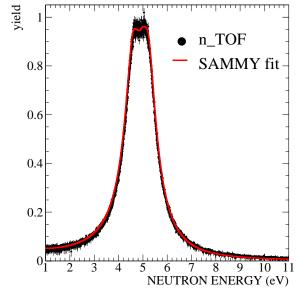
FIG. 5: (Color online) R-matrix fit of the background subtracted yield of the first resonance in ^{197}Au. Normalization at 25 keV [39] leads to a predicted value of 0.973 ± 0.010 at 4.9 eV in perfect agreement with the SAMMY fit with the resonance parameters of Ref. [18], which gives 0.971 ± 0.019.

with the Si-monitor and a calibrated fission chamber [40].

D. Multiple scattering and isotopic impurities

In the unresolved region, neutron multiple scattering and self shielding corrections in the sample have been determined with the SESH code [41]. In the RRR these corrections were included in the SAMMY analysis. The results from the continuum region and from the RRR are converging in the neutron energy range from 1.5 to 3 keV within uncertainties. The multiple scattering corrections were below 4 and 5% for the even and odd isotopes with uncertainties of about 10%.

Isotopic corrections have been applied by subtracting the contributions from the contaminants at all energies. The effect of the PHWT has been taken into account in the isotopic correction by weighting the cross sections of the contaminants with the ratio of the neutron separation energies of the main isotope and of the contaminants. The code for isotopic corrections was validated by tests with cross sections from a database, which were artificially contaminated with several impurities. The contributions of ^{190,192}Os were considered by the cross section data of Browne and Berman [16], which have been confirmed at 25 keV by a recent activation measurement [42]. At higher energies, these data were extrapolated by means of the energy dependence adopted from the JEFF-3.1 evaluation [43]. Because of their smaller cross sections ^{190}Os and ^{192}Os contribute only a rather small part to the correction. The more significant contribution

of ^{189}Os was obtained with the cross sections of Winters *et al.* [44], which are in good agreement with recent results between 5 and 90 keV [17]. The experimental data [44] were also extrapolated to higher neutron energies by means of the JEFF-3.1 evaluation.

The related systematic uncertainties have been estimated by variation of the cross section within uncertainties. On average, the uncertainties due to isotopic corrections were 1.5, 0.7, and 0.7% for ^{186}Os, ^{187}Os, and ^{188}Os, respectively.

IV. RESULTS

The (n, γ) cross sections of ^{186}Os, ^{187}Os, and ^{188}Os have been measured with high resolution in the energy range from a few eV to 1 MeV. The results for the resolved resonance region up to a few keV, which has been analyzed with the R-matrix code SAMMY, will be reported separately in Paper III [29] together with the determination of Maxwellian average cross sections and with the calculation of stellar enhancement factors for the s-process analysis in the W-Re-Os region.

In the unresolved resonance region of interest here, the results have been averaged over 20 bins per decade for comparison with previous results [15–17] in Fig. 6. In case of the ^{187}Os cross section good agreement is found among all data sets, but there are clear discrepancies in the results for ^{186}Os and ^{188}Os, where the present values are significantly lower and exhibit a more pronounced competition by inelastic scattering channels corresponding to the first excited states at 137 and 155 keV.

The ^{188}Os cross section shows the largest discrepancies, presumably because the high energy part of the spectrum was over-weighted in the PHWT applications of the previous measurements as outlined in Ref. [45]. To reproduce the previous ^{188}Os cross section values from our data would require to reduce the background in the keV region by 30%, far beyond any justifiable solution.

Numerical values of the data points in Fig. 6 are listed in Table II.

A detailed account of the Hauser-Feshbach statistical model (HFSM) calculations performed for the Re/Os clock will be presented in Paper III [29] with a discussion of the various parameters deduced from the resonance analyses and from the (n, n') cross section measurement in Paper II [46].

V. MAXWELLIAN AVERAGES

The cross section results from the continuum region (Table II) were complemented below 3 keV for ^{186}Os and ^{188}Os and below 2 keV for ^{187}Os by average cross sections with a resolution of 20 bins per decade, which were extracted from the resonance parameters as reported in Paper III. From these values, MACS have been calculated
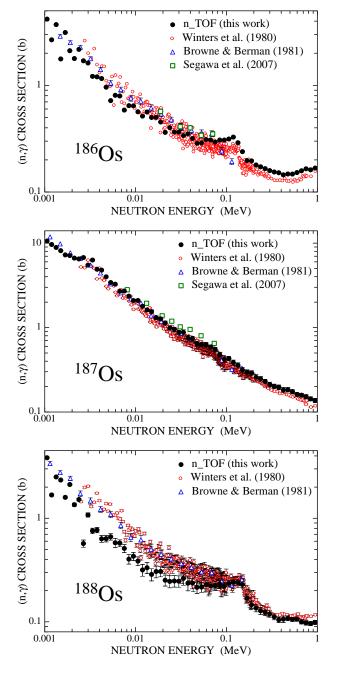
FIG. 6: (Color online) Comparison between the present results and data of Winters *et al.* [15], Browne and Berman [16], and Segawa *et al.* [17]. The present data are averaged over 20 bins per energy decade.

according to

$$\langle\sigma\rangle_{kT} = \frac{2}{\sqrt{\pi}} \frac{\int_0^\infty \sigma(E_n)\ E_n\ \mathrm{e}^{-E_n/kT}\ dE_n}{\int_0^\infty E_n\ \mathrm{e}^{-E_n/kT}\ dE_n}. \quad (2)$$

for thermal energies from 5 to 100 keV.

At the lowest thermal energies, the results shown in Fig. 7 and summarized in Table III benefit from the fact that a complete set of resonance parameters was avail-

able for the first time. The total uncertainties of the MACS, which are below 4.3%, 3.3%, and 4.7% for ^{186}Os, ^{187}Os, and ^{188}Os, respectively, are clearly dominated by the systematic uncertainties given in Table IV.
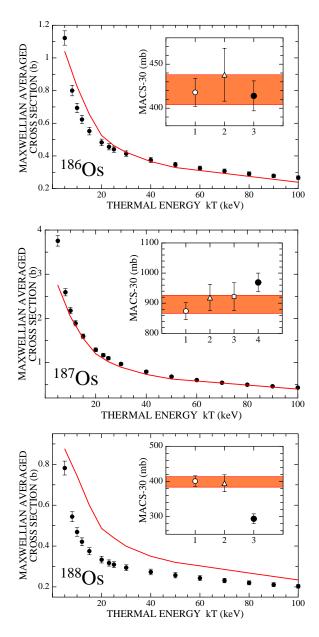

FIG. 7: (Color online) Present Maxwellian averaged cross sections (solid circles with error bars) compared with the previously recommended values of Bao *et al.* [48] (solid line). The insets focus on the values at $kT = 30$ keV, which are commonly used for comparison. At this energy the present uncertainties are 4.1, 3.2, and 4.7% for ^{186}Os, ^{187}Os, and ^{188}Os, respectively. Experimental results refer to the work of Winters *et al.* [15] (open circles), Browne and Berman [16] (triangles), and Bokhovko *et al.* [47] (open square). The values of Bao *et al.* [48] are indicated by shaded bars.

The comparison of the present results in Fig. 7 with the recommended values of Bao *et al.* [48], which are

based on previously reported MACSs [15, 16, 47], shows large discrepancies for ^{188}Os as expected from the cross section plot in Fig. 6. Differences for the even isotopes ^{186,188}Os are smaller and are found mostly below thermal energies of 25 keV. This is reflected by the values for $kT = 30$ keV, which are plotted in the insets of Fig. 7. The significant difference in case of ^{187}Os implies that the cross section ratio $\langle\sigma\rangle_{186}/\langle\sigma\rangle_{187}$ is now 11% smaller than obtained from the previously recommended values [48]. At thermal energies around $kT = 23$ keV, where the s-process abundances in thermally pulsing low mass AGB stars are actually shaped [20], the ratio is even 19% smaller than recommended in Ref. [48].

Although the differences between the individual cross sections and previous data are practically within the quoted uncertainties, it was renounced to combine all existing results in a single data set as one would do in a typical cross section evaluation. Instead of determining the cross section ratio $\langle\sigma\rangle_{186}/\langle\sigma\rangle_{187}$ - which is in fact the relevant quantity required for the Re/Os clock (Eq. 1) - after combining all existing results into separate data sets, it is preferable to maintain the internal consistency provided by the present experiment. This offers the advantage that systematic uncertainties in the measurement and data analysis may, at least partly, cancel out in the cross section ratio. In other words, the 5% uncertainty of the cross section ratio at $kT = 25$ keV obtained from the MACS in Table III represents a safe upper limit.

In summary, the present MACS values are leading to a considerable reduction of the s-process abundance of ^{187}Os. This reduction of the s-process part results in a larger radiogenic component of ^{187}Os and in a correspondingly older ^{187}Re age.

A. Discussion of uncertainties

The statistical uncertainties are essentially determined by the signal/background ratio in the TOF spectra (Fig. 3). Due to the background from in-beam γ-rays, the statistical uncertainties are largest in the astrophysically relevant region from 1 to 100 keV, but the corresponding contributions to the total MACS uncertainties are always below 2.3%.

The systematic uncertainties have been discussed before and are summarized in Table IV.

VI. CONCLUSIONS

The present work (Paper I) is part of an experimental effort for a revision of the Re/Os cosmo-chronometer. It describes the measurement of the neutron capture cross sections of ^{186,187,188}Os at the CERN n_TOF facility with improved accuracy and over a wide energy range of neutron energies from 1 eV to 1 MeV. From these data Maxwellian averaged cross sections were obtained with uncertainties between 3 and 4%. These results were complemented by a measurement of the inelastic scattering cross section of ^{187}Os at FZK (Paper II) and by a detailed resonance analysis of the Os cross sections (Paper III). The combined information represents a complete data set describing the neutron physics part of the Re/Os clock.

TABLE II: Averaged neutron capture cross sections[a] and total uncertainties of ^{186}Os, ^{187}Os, and ^{188}Os.

Energy (keV)	Range (keV)	(n, γ) cross sections (mbarn)		
		^{186}Os	^{187}Os	^{188}Os
1.06	1.00 - 1.12	3709 ± 72	12316 ± 178	4088 ± 47
1.19	1.12 - 1.26	3696 ± 71	12315 ± 172	1625 ± 44
1.34	1.26 - 1.41	3510 ± 71	9109 ± 167	2780 ± 47
1.50	1.41 - 1.58	1982 ± 68	8887 ± 162	2374 ± 50
1.68	1.58 - 1.78	3097 ± 76	7215 ± 150	1705 ± 44
1.89	1.78 - 2.00	2481 ± 71	8105 ± 156	2245 ± 48
2.12	2.00 - 2.24	1972 ± 68	6558 ± 144	1520 ± 48
2.37	2.24 - 2.51	2194 ± 71	6450 ± 143	1720 ± 47
2.67	2.51 - 2.82	1748 ± 67	6744 ± 144	836 ± 46
2.99	2.82 - 3.16	1711 ± 68	5510 ± 134	1093 ± 49
3.36	3.16 - 3.55	1226 ± 65	6314 ± 139	758 ± 46
3.76	3.55 - 3.98	1214 ± 63	4917 ± 125	771 ± 45
4.22	3.98 - 4.47	1170 ± 65	4802 ± 124	635 ± 47
4.74	4.47 - 5.01	975 ± 59	4005 ± 113	638 ± 45
5.32	5.01 - 5.62	733 ± 59	3430 ± 110	665 ± 47
5.97	5.62 - 6.31	821 ± 75	3280 ± 110	583 ± 59
6.69	6.31 - 7.08	810 ± 57	2705 ± 94	578 ± 44
7.51	7.08 - 7.94	601 ± 56	2722 ± 95	514 ± 45
8.43	7.94 - 8.91	659 ± 54	2366 ± 88	406 ± 42
9.46	8.91 - 10.0	658 ± 49	2101 ± 82	433 ± 39
10.6	10.0 - 11.2	580 ± 48	2102 ± 81	389 ± 37
11.9	11.2 - 12.6	529 ± 53	1800 ± 80	319 ± 41
13.4	12.6 - 14.1	577 ± 53	1627 ± 77	336 ± 41
15.0	14.1 - 15.9	514 ± 49	1560 ± 73	289 ± 38
16.8	15.9 - 17.8	513 ± 50	1324 ± 70	308 ± 40
18.9	17.8 - 20.0	464 ± 44	1278 ± 64	309 ± 34
21.2	20.0 - 22.4	372 ± 40	1142 ± 61	254 ± 31
23.8	22.4 - 25.1	410 ± 40	999 ± 57	247 ± 33
26.7	25.1 - 28.2	373 ± 40	961 ± 55	249 ± 31
29.9	28.2 - 31.6	370 ± 39	879 ± 54	248 ± 30
33.6	31.6 - 35.5	343 ± 47	880 ± 63	263 ± 37
37.7	35.5 - 39.8	355 ± 45	758 ± 56	237 ± 37
42.2	39.8 - 44.7	321 ± 35	740 ± 49	237 ± 28
47.4	44.7 - 50.1	288 ± 33	646 ± 45	216 ± 27
53.2	50.1 - 56.2	290 ± 29	626 ± 40	217 ± 24
59.7	56.2 - 63.1	310 ± 26	628 ± 37	229 ± 21
67.0	63.1 - 70.8	307 ± 24	586 ± 34	222 ± 19
75.1	70.8 - 79.4	293 ± 28	547 ± 36	224 ± 23
84.3	79.4 - 89.1	305 ± 26	474 ± 33	232 ± 21
94.6	89.1 - 100	305 ± 25	420 ± 31	219 ± 20

[a] 20 bins per energy decade.

Energy (keV)	Range (keV)	(n, γ) cross sections (mbarn)		
		^{186}Os	^{187}Os	^{188}Os
106	100 - 112	311 ± 20	428 ± 27	234 ± 16
119	112 - 126	325 ± 21	381 ± 28	240 ± 17
134	126 - 141	287 ± 18	356 ± 24	238 ± 15
150	141 - 158	236 ± 18	311 ± 24	228 ± 15
168	158 - 178	194 ± 18	292 ± 21	168 ± 15
189	178 - 200	193 ± 13	287 ± 18	146 ± 11
212	200 - 224	179 ± 14	258 ± 19	136 ± 11
238	224 - 251	171 ± 13	245 ± 17	128 ± 10
267	251 - 282	164 ± 11	229 ± 15	124 ± 9
299	282 - 316	158 ± 10	211 ± 13	119 ± 8
336	316 - 355	153 ± 9	201 ± 12	112 ± 7
376	355 - 398	151 ± 8	196 ± 12	105 ± 6
422	398 - 447	145 ± 9	182 ± 13	106 ± 7
474	447 - 501	148 ± 8	184 ± 11	108 ± 6
532	501 - 562	147 ± 7	174 ± 9	106 ± 5
597	562 - 631	152 ± 6	161 ± 9	106 ± 5
669	631 - 708	158 ± 7	158 ± 8	100 ± 5
751	708 - 794	165 ± 7	152 ± 8	98 ± 5
843	794 - 891	161 ± 7	144 ± 8	96 ± 5
946	891 - 1000	167 ± 6	137 ± 8	99 ± 5

[a] 20 bins per energy decade.

TABLE III: Maxwellian averaged cross sections for the ground state (obtained from experimental data).

Thermal energy (keV)	MACS (mb)		
	^{186}Os	^{187}Os	^{188}Os
5	1122±44	3755±118	782±34
8	800±32	2592±83	544±24
10	694±28	2176±70	469±21
12	623±26	1890±61	421±19
15	552±23	1596±53	375±17
20	483±20	1291±42	333±16
23	456±19	1168±39	317±15
25	441±19	1100±37	309±14
30	414±17	969±32	294±14
40	375±16	794±27	273±14
50	347±14	683±23	257±13
60	325±13	605±21	243±12
70	307±13	545±19	231±11
80	291±12	500±18	220±10
90	278±11	464±15	211±10
100	267±11	434±14	203±9

TABLE IV: Systematic and statistical uncertainties of the MACS.

Source of uncertainty	Uncertainty (%)		
	^{186}Os	^{187}Os	^{188}Os
PHWT	2.0	2.0	2.0
Neutron flux	2.0	2.0	2.0
Background subtraction	2.0	1.0	3.0
Isotopic impurities	1.5	0.7	0.7
Multiple scattering	0.4	0.5	0.4
Counting statistics[a]	1.5	1.0	2.0
Total	4.1	3.3	4.7

[a] for $kT = 30$ keV

[1] M. Galeazzi, F. Fontanelli, F. Gatti, and S. Vitale, Phys. Rev. C **63**, 014302 (2000).
[2] D.D. Clayton, Ap. J. **139**, 637 (1964).
[3] C. Sneden, A. McWilliam, G.W. Preston, J.J. Cowan, D.L. Burris, and B.J. Armosky, Ap. J. **467**, 819 (1996).
[4] C. Sneden, J. Cowan, D. Burris, and J. Truran, Ap. J. **496**, 235 (1998).
[5] C. Sneden *et al.*, Ap. J. **591**, 936 (2003).
[6] W.L. Freedman *et al.*, Ap. J. **553**, 47 (2001).
[7] L.M. Krauss and B. Chaboyer, Science **299**, 65 (2003).
[8] C.L. Bennett *et al.*, Ap. J. Suppl. **148**, 1 (2003).
[9] F. Käppeler, S. Jaag, Z. Bao, and G. Reffo, Ap. J. **366**, 605 (1991).
[10] K. Sonnabend *et al.*, Ap. J. **583**, 506 (2003).
[11] P. Mohr, S. Goriely, T. Shizuma, and T. Hayakawa, in *Nuclei in the Cosmos IX*, edited by A. Mengoni and *et al.* (Proceedings of Science, Trieste, 2007), pp. PoS(NIC–IX)142, http://pos.sissa.it.
[12] F. Bosch *et al.*, Phys. Rev. Lett. **77**, 5190 (1996).
[13] K. Takahashi, in *Tours Symposium on Nuclear Physics III*, edited by M. Arnould *et al.* (AIP, New York, 1998), pp. 616 – 625.
[14] T. Shizuma *et al.*, Phys. Rev. C **72**, 025808 (2005).
[15] R.R. Winters, R.L. Macklin, and J. Halperin, Phys. Rev. C **21**, 563 (1980).
[16] J.C. Browne and B.L. Berman, Phys. Rev.C **23**, 1434 (1981).
[17] M. Segawa, T. Masaki, Y. Nagai, Y. Temma, T. Shima, K. Mishima, M. Igashira, S. Goriely, A. Koning, and S. Hilaire, Phys. Rev. C **76**, 022802(R) (2007).
[18] S.F. Mughabghab, in *Atlas of Neutron Resonances, 5th Edition* (Elsevier, Amsterdam, 2006).
[19] M. Busso, R. Gallino, and G.J. Wasserburg, Ann. Rev. Astron. Astrophys. **37**, 239 (1999).
[20] R. Gallino, C. Arlandini, M. Busso, M. Lugaro, C. Travaglio, O. Straniero, O. A. Chieffi, and M. Limongi, Ap. J. **497**, 388 (1998).
[21] R.L Hershberger, R.L. Macklin, M. Balakrishnan, N.W. Hill, and M.T. McEllistrem, Phys. Rev. C **28**, 2249 (1983).
[22] R.L. Macklin, R.R. Winters, N.W. Hill, and J.A. Harvey, Ap. J. **274**, 408 (1983).
[23] L. Litvinsky, A. Murzin, and A. Shkarupa, Phys. At. Nucl. **56**, 17 (1993).
[24] L. Litvinsky *et al.*, Phys. At. Nucl. **58**, 164 (1995).
[25] U. Abbondanno *et al.*, Technical report, CERN, Geneva, Switzerland, (unpublished), report CERN-SL-2002-053 ECT.
[26] R. Plag, M. Heil, F. Käppeler, P. Pavlopoulos, R. Rei-

farth, and K. Wisshak, Nucl. Instr. Meth. A **496**, 425 (2003).
[27] S. Marrone and *et al.*, Nucl. Instr. Meth. Phys. Res. A **517**, 389 (2004).
[28] M. Mosconi, Ph.D. thesis, University of Karlsruhe, 2007.
[29] K. Fujii, M. Mosconi, A. Mengoni, *et al.*, Phys. Rev. C (in preparation).
[30] R.L. Macklin and J.H. Gibbons, Phys. Rev. **159**, 1007 (1967), includes H. Maier-Leibnitz, priv. comm. and Rau63.
[31] G. Aerts, E. Berthoumieux, F. Gunsing, and L. Perrot, Technical report, CEA Saclay, France, (unpublished), dAPNIA-04-106.
[32] R. Terlizzi, private communication (unpublished).
[33] S. Marrone and *et al.*, Phys. Rev. C **73**, 034604 (2006).
[34] R. Terlizzi, Phys. Rev. C **75**, 035807 (2007).
[35] J. Apostolakis, Technical report, CERN, GEANT library, (unpublished), http://wwwinfo.cern.ch/asd/geant/.
[36] C. Borcea and *et al.*, Nucl. Instr. Meth. Phys. Res. A **513**, 524 (2003).
[37] R.L. Macklin, J. Halperin, and R.R. Winters, Nucl. Instr. Meth. A **164**, 213 (1979).
[38] N. Larson, Technical report, Oak Ridge National Laboratory (unpublished).
[39] W. Ratynski and F. Käppeler, Phys. Rev. C **37**, 595 (1988).
[40] C. Domingo-Pardo, Ph.D. thesis, CSIC-University of Valencia, 2005.
[41] F. Fröhner, Technical report, Gulf General Atomic, GA-8380 (unpublished).
[42] J. Marganiec *et al.*, Phys. Rev. C in preparation (2009).
[43] JEFF-3.1 General Purpose Neutron File, (OECD Nuclear Energy Agency, Paris, 2005) On-Line access: http://www.nea.fr/html/dbdata/JEFF/.
[44] R.R. Winters, R.L. Macklin, and R.L. Hershberger, Astron. Astrophys. **171**, 9 (1987).
[45] M. Sowerby and F. Corvi, in *Nuclear Data for Science and Technology*, edited by S. Igarasi (Saikon, Tokyo, 1988), p. 37.
[46] M. Mosconi, M. Heil, F. Käppeler, R. Plag, and A. Mengoni, Phys. Rev. C (in preparation).
[47] M. Bokhovko *et al.*, in *Nuclear Data for Science and Technology, Research Reports in Physics*, edited by S. Qaim (Springer, Berlin, 1992), p. 62.
[48] Z.Y. Bao, H. Beer, F. Käppeler, F. Voss, K. Wisshak, and T. Rauscher, Atomic Data Nucl. Data Tables **76**, 70 (2000).